

Efficient and Robust Video Defense Framework against 3D-field Personalized Talking Face

Rui-qing Sun^{1,†} Xingshan Yao^{1,†} Tian Lan² Hui-Yang Zhao¹ Jia-Ling Shi¹ Chen-Hao Cui¹
Zhijing Wu¹ Chen Yang^{1,*} Xian-Ling Mao^{1,*}

¹Beijing Institute of Technology

²Alibaba International Digital Commerce

Abstract

State-of-the-art 3D-field video-referenced Talking Face Generation (TFG) methods synthesize high-fidelity personalized talking-face videos in real time by modeling 3D geometry and appearance from reference portrait video. This capability raises significant privacy concerns regarding malicious misuse of personal portraits. However, no efficient defense framework exists to protect such videos against 3D-field TFG methods. While image-based defenses could apply per-frame 2D perturbations, they incur prohibitive computational costs, severe video quality degradation, failing to disrupt 3D information for video protection. To address this, we propose a novel and efficient video defense framework against 3D-field TFG methods, which protects portrait video by perturbing the 3D information acquisition process while maintain high-fidelity video quality. Specifically, our method introduces: (1) a similarity-guided parameter sharing mechanism for computational efficiency, and (2) a multi-scale dual-domain attention module to jointly optimize spatial-frequency perturbations. Extensive experiments demonstrate that our proposed framework exhibits strong defense capability and achieves a 47× acceleration over the fastest baseline while maintaining high fidelity. Moreover, it remains robust against scaling operations and state-of-the-art purification attacks, and the effectiveness of our design choices is further validated through ablation studies. Our project is available at <https://github.com/Richen7418/VDF>.

1. Introduction

Recent advances in 3D-field video-referenced Talking Face Generation (TFG) methods leverage 3D neural fields to capture and store a individual’s comprehensive geometric and appearance information from a short reference video

during training [1, 5, 10, 12, 18, 28, 44]. Compared to image-referenced TFG approaches [16, 27], these 3D field-based methods synthesize high-fidelity personalized videos at over 30 frames per second (FPS) while enabling precise control of head poses and facial dynamics through additional motion parameters. Consequently, significant privacy concerns have emerged regarding malicious exploitation of such systems—particularly when driven by toxic text prompts or harmful audio inputs to synthesize non-consensual portrait videos.

However, to the best of our knowledge, defenses specifically designed for 3D-field video-referenced TFG methods remain largely unexplored. Intuitively, a simple solution is to decompose an reference portrait video into individual frames and apply image-level defenses frame-by-frame [8, 20, 21, 33, 42] developed for general image-based TFG models. Unfortunately, this defense approach suffers from four critical limitations against 3D-field TFG methods: (1) **Efficiency**: Frame-by-frame defense leads to extremely low efficiency, which makes it impractical for real-world use; (2) **Robustness**: Video transmission operations such as resizing and color compression [34] can easily destroy spatial-domain perturbations injected by existing image-based defense methods, and purification methods designed to remove harmful noise in images can also eliminate these perturbations [23, 26, 48]; (3) **Effectiveness**: They cannot apply effective perturbation on frequency video information, leading to worse protection performance, as illustrated in Fig 1; and (4) **Visual Quality**: Defended videos exhibit poor visual quality due to the numerous perturbation on spatial-domain. In summary, a practically useful video defense framework should achieve high efficiency, robustness to scaling and purification, defense effectiveness and high visual quality.

To achieve this goal, we propose a novel and efficient video defense framework against 3D-field TFG methods. Specifically, our framework overcomes the weaknesses of image-based defense framework by introducing several key designs: (1) **Defense Efficiency**: We design a similarity-

[†]Equal contribution. ^{*}Corresponding author.

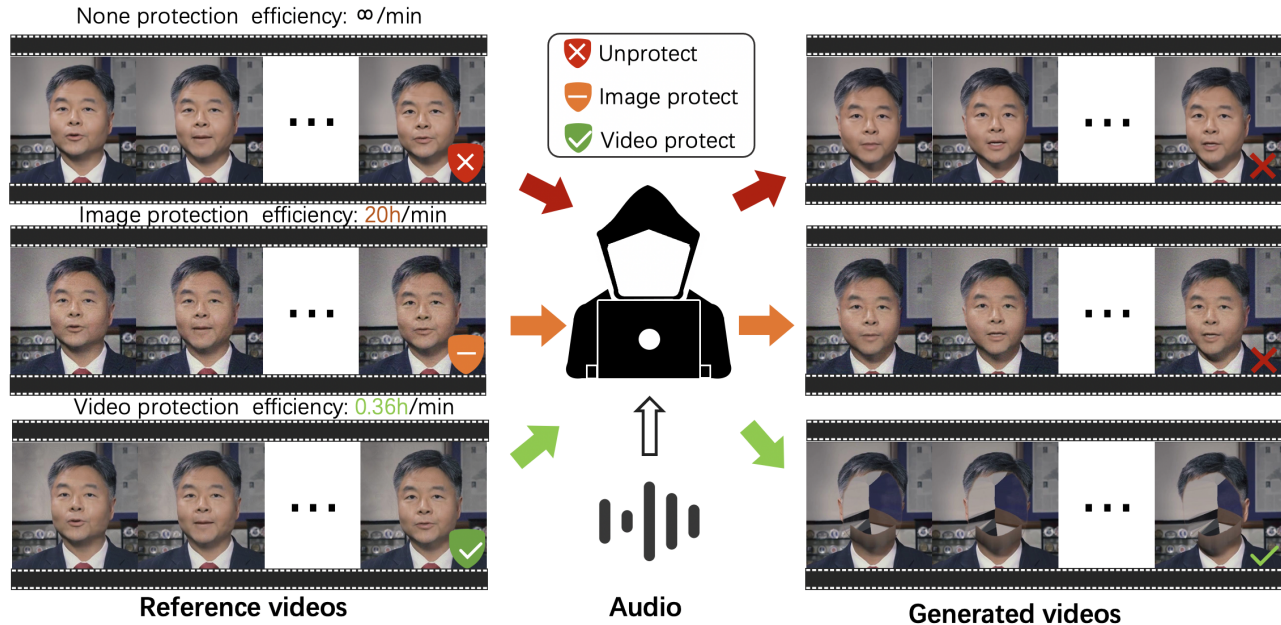


Figure 1. **Motivation illustration.** Given an audio input and a reference video, 3D field-based TFG models can synthesize highly realistic personalized talking-face videos. However, decomposing a video into individual frames and applying existing 2D image-level defenses introduces substantial computational overhead while proving largely ineffective against 3D-based generation. To efficiently protect portrait privacy from such personalized TFG models, we propose a video-level defense framework (VDF) that achieves both high efficiency and strong robustness.

guided parameter sharing mechanism, which reduces computational costs while maintaining visual quality; (2) **Defense Effectiveness and Robustness:** We first introduce effective perturbation using frequency domain perturbation rather than the spatial domain perturbations, which also exhibit better robustness against scale variations and color [11, 46] and purification models. Then, we design a multi-scale optimization strategy that refines perturbations under varying resolution conditions to further strengthen robustness against scaling such as resizing and color compression; and (3) **Visual Quality:** An additional spatial-domain attention mechanism is designed to adaptively suppresses redundant pixel-level perturbations, As the global nature of frequency-domain perturbations inevitably introduces some noise redundancy.

Following prior work, we conduct extensive experiments to evaluate our method on a corresponding personalized TFG dataset [28, 44]. Experimental results demonstrate several important findings: (1) Compared with conventional image-based generalized TFG defenses or spatial-domain method, our proposed framework effectively resists attacks from 3D-field based personalized TFG models while maintaining high visual quality (Section and Section); (2) Our proposed method exhibit powerful robustness to scaling operations and state-of-the-art purification models like JPEG [34], DiffPure [23] and FreqPure [26] (Section 4.4);

and (3) Computational cost is much lower than baselines, achieving 60x acceleration. In summary, our main contributions are four-fold:

- We identify four essential properties that a practical portrait video defense method against 3D-field TFG methods should possess: high computational efficiency, robustness to video scaling and purification, defense effectiveness and high-fidelity visual quality.
- We extend and evaluate several state-of-the-art generalized TFG defense methods against 3D-field TFG, and extensive experimental results demonstrate that existing approaches fail to defend against 3D field-based personalized TFG attacks and lack scalability for large-scale practical deployment.
- We propose a novel and efficient defense framework to achieve achieving robust protection against 3D field-based TFG attacks while preserving high video quality.
- Extensive experiments validate that our framework achieves privacy protection at a relatively low computational cost and exhibits strong resilience against purification-based attacks.

2. Related Work

3D field-based Talking Face Generation. Talking Face Generation aims to synthesize realistic portrait videos of a

target subject speaking arbitrary content. Early TFG methods mainly focused on building generic generative models, such as GAN-based frameworks, that could animate any static portrait using a reference image once the model is trained [2, 4, 31]. However, these image-based models often struggled to produce natural and believable facial motions. With recent advances in 3D reconstruction, 3D representation techniques based on NeRF [1, 12, 17] and 3D Gaussian Splatting (3DGS) [5, 19, 47] have significantly boosted the development of video-based TFG. Unlike generic image-based TFG models trained on large-scale datasets, 3D field-based methods learn the 3D geometry and appearance of a specific person from a few minutes of reference video, enabling more realistic and high-fidelity synthesis. For instance, ER-NeRF [17] improves rendering efficiency by encoding spatial coordinates via tri-plane hash encoding, yet it still suffers from the average-lip problem. GeneFace [44] mitigates this issue by generating lip landmarks instead of directly using audio features, though this compromises the accuracy of lip synchronization. SyncTalk [28] achieves more precise lip motion and head pose generation by refining reference video processing and introducing a high-quality audio encoder.

3DGS-based methods further advance personalized TFG by modeling facial motion through continuous Gaussian splatting, enabling smooth and persistent geometric deformation. Recently proposed TalkingGaussian [18] and GaussianTalker [5] methods enhance lip structure preservation and visual detail, achieving stable and real-time rendering through shared implicit Gaussian attribute encoding. Subsequently, SyncTalk++ [29] integrates a Face-Sync Controller and a 3D facial blendshape model to achieve highly controllable head and expression dynamics. While these high-fidelity portrait generation techniques mark a major milestone in personalized synthesis, they have also sparked growing concerns over portrait privacy. Widely adopted video processing pipelines in the domain are selected as the targets of our defense [5, 17, 19, 28, 35, 39, 43]. Both SyncTalk and SyncTalk++ can generate highly realistic videos that are almost indistinguishable from real ones, with SyncTalk++ requiring longer reference videos due to its 3DGS-based reconstruction process. Considering that baseline video defense algorithms typically require dozens of hours to protect a one-minute video, we adopt SyncTalk as our representative personalized TFG model.

Purification. Image purification has emerged as a critical defense mechanism in computer vision systems against adversarial attacks, with the primary objective of eliminating adversarial perturbations while preserving the essential semantic content of images [7, 9, 14, 23, 25, 34, 37, 41, 45]. Early studies demonstrated that straightforward image pre-processing techniques, such as image compression (e.g., JPEG encoding [34]) and resizing [41]), could partially mit-

igate certain types of adversarial noise. These methods have garnered significant attention because of their computational efficiency and the fact that they do not require modifications to the underlying model. In recent years, with the rapid advancement of generative models, purification approaches based on diffusion models have achieved remarkable success. Diffusion models inherently possess a strong “re-purification” capability due to their generative process, which involves progressively adding and removing noise. This approach effectively removes complex targeted adversarial perturbations, as adversarial noise is typically diluted and overwritten during multiple iterations of noise addition and removal [37, 45]. DiffPure[23] was the first to apply a pre-trained diffusion model for adversarial purification, leveraging its forward noising and reverse denoising process to effectively restore adversarial examples to the clean image manifold. From a frequency-domain perspective, FreqPure[25] selectively preserves the low-frequency components of the adversarial image that remain intact, thus achieving purification while better maintaining the original semantic structure of the image. In the experiments, various real-world degradations, including resizing, JPEG compression [34], and purification methods such as DiffPure [23] and FreqPure [26], are employed to evaluate the purification robustness of our framework and demonstrate its practicality.

3. Method

3.1. Preliminary

3.1.1. 3D Field-based Audio-driven Talking Face Generation

Given a reference portrait video and an input audio, the goal of personalized TFG is to generate a high-fidelity talking video of the target person synchronized with the speech audio. To make the generated video more natural and realistic, recent works based on 3D fields typically adopt NeRF or 3DGS models as the underlying architecture, pre-learning and storing the 3D information for the target person, as demonstrated in Fig 3. Following the volumetric rendering formulation, the color of a pixel is computed by integrating the emitted radiance along the corresponding camera ray:

$$\hat{C}(\mathbf{r}) = \int_{t_n}^{t_f} \sigma(\mathbf{r}(t)) \cdot \mathbf{c}(\mathbf{r}(t), \mathbf{d}, \mathbf{e}, \mathbf{a}) \cdot T(t) dt, \quad (1)$$

where $\mathbf{r}(t) = \mathbf{o} + t\mathbf{d}$ denotes a ray originating from the camera center \mathbf{o} and extending along the direction \mathbf{d} with depth t . Here, $\sigma(\mathbf{r}(t))$ represents the volume density (opacity) at position $\mathbf{r}(t)$, and $\mathbf{c}(\mathbf{r}(t), \mathbf{d}, \mathbf{e}, \mathbf{a})$ is the emitted color conditioned on viewing direction \mathbf{d} , facial expression parameters \mathbf{e} , and audio feature \mathbf{a} . $T(t) = \exp(-\int_{t_n}^t \sigma(\mathbf{r}(s)) ds)$ denotes the accumulated transmittance from near bound t_n to depth t , modeling light attenuation along the ray. This

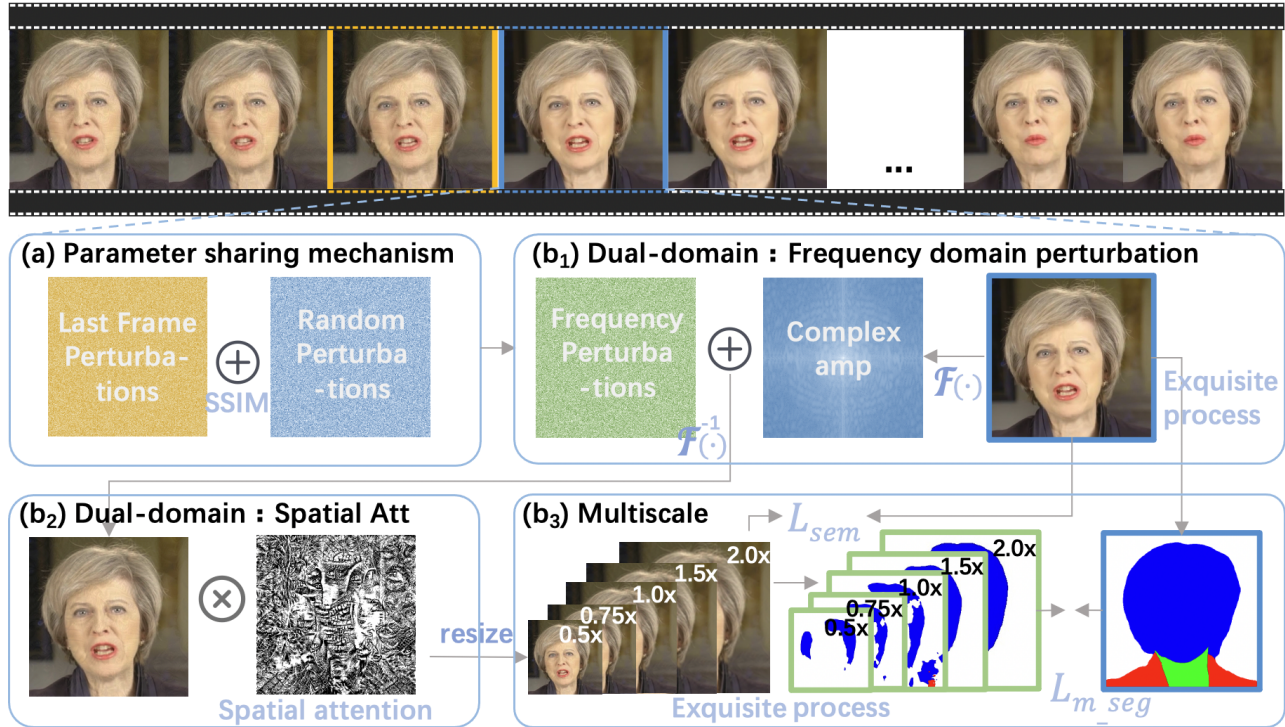


Figure 2. Overall architecture of the proposed framework. (a) Efficiency improvement mechanism. (b) Dual-domain attention mechanism with multiscale module.

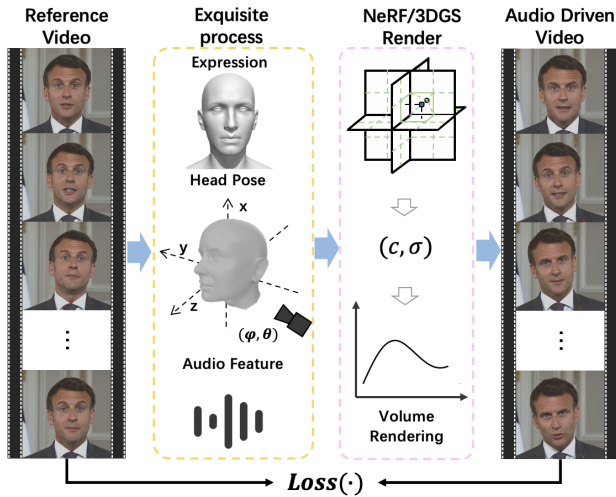


Figure 3. The basic process of acquiring target-specific information in 3D field-based TFG models. Accurate identity reconstruction relies heavily on the exquisite processing of the reference video, where expressions, head poses, and audio features are extracted and then rendered via NeRF or 3DGS to synthesize an audio-driven talking-face video.

formulation jointly captures geometry (σ) and appearance (c) in an end-to-end differentiable manner, enabling the

model to learn dynamic face geometry and view-dependent appearance for high-fidelity audio-synchronized rendering. Since the model incorporates explicit physical processes, it only requires the continuous update of a small number of trainable parameters, allowing the generated video frames to progressively match the reference video frames. This enables the model to acquire 3D information of the target person and learn the end-to-end mapping between audio, facial expression parameters, and facial deformations. Compared to image-based method, which require iterative denoising, the 3D field-based method allows for real-time video output while ensuring precise control of the person's pose and maintaining high identity consistency.

3.1.2. Adversarial Examples for Image-based Talking Face Generation

Previous defense approaches have primarily focused on image-based TFG models. These methods protect identity privacy by introducing carefully designed perturbations to the portrait images, misleading the latent diffusion model to learn incorrect representations, thereby degrading the visual quality of the generated talking-face videos. Most prior works achieve this goal by exploiting vulnerabilities in the diffusion process through three types of objective functions:

- Semantic loss is adopted as one of the objective functions during the training of LDM models. Increasing the value

of the semantic loss forces the generated results to deviate from the intended semantics, thereby reducing the model’s ability to produce faithful and coherent outputs:

$$\mathcal{L}_S = -\mathbb{E}_{t,\epsilon,\mathbf{z}_t} \|\epsilon - \epsilon_\theta(\mathbf{z}_t, t)\|_2^2, \quad (2)$$

Where \mathcal{L}_S denotes the semantic loss term, and $\mathbb{E}_{t,\epsilon,\mathbf{z}_t}$ represents the expectation over the diffusion timestep t . ϵ is the ground-truth Gaussian noise sampled from $\mathcal{N}(0, I)$, while $\epsilon_\theta(\mathbf{z}_t, t)$ denotes the noise predicted by the denoising network parameterized by θ at timestep t . \mathbf{z}_t is the latent variable at diffusion step t , obtained by perturbing the original latent representation with Gaussian noise. Finally, $\|\cdot\|_2^2$ represents the squared L2 norm used to measure the Euclidean distance between two noise vectors.

- Texture loss focuses on the latent-level representation of images. It constrains the model’s ability to extract the target person’s distinctive portrait characteristics by forcing the latent embedding of the input image x to align with that of another image y extracting by VAE encoder $\mathcal{E}(\cdot)$:

$$\mathcal{L}_T = \|\mathcal{E}(x) - \mathcal{E}(y)\|_2^2, \quad (3)$$

- The silence loss aims to eliminate the driving effect of audio signals on portrait generation. By aligning the output of the LDM model with its input, it ensures that the generated video remains unchanged under different speech inputs, keeping the target portrait motionless and silent:

$$\mathcal{L}_N = \mathbb{E}_{t,\epsilon} \mathbb{E}_{\mathcal{E}(p), p, a_i, \epsilon, t} \left[\|\epsilon - \epsilon_\theta(\hat{z}_t, t, p, a_i)\|_2^2 \right], \quad (4)$$

Where $\mathbb{E}_{t,\epsilon}$ and $\mathbb{E}_{\mathcal{E}(p), p, a_i, \epsilon, t}$ indicate the expectation over diffusion timesteps, noise, and conditional variables. $\epsilon_\theta(\hat{z}_t, t, p, a_i)$ represents the noise predicted by the LDM conditioned on the portrait p and audio a_i , and \hat{z}_t is the noised latent representation at timestep t .

The final adversarial loss \mathcal{L}_{adv} can be composed of any combination of the semantic loss, texture loss, and silence loss, or alternatively, any one of them individually. Then the PGD[22] algorithm is utilized to craft adversarial examples through an iterative gradient descent optimization process:

$$x^n = \mathcal{P}_{B_\infty(x, \delta)} \left[x^{n-1} - \eta \text{sign}(\nabla_{x^{n-1}} \mathcal{L}_{adv}(x^{n-1})) \right] \quad (5)$$

Where x^n represents the updated sample after the n -th iteration, and x^{n-1} is the result from the previous step. $\mathcal{P}_{B_\infty(x, \delta)}[\cdot]$ denotes the projection operator that constrains the updated sample within an L_∞ ball of radius δ centered at x . η is the step size controlling the magnitude of each update, and $\text{sign}(\cdot)$ extracts the element-wise sign of the gradient. $\nabla_{x^{n-1}} \mathcal{L}_{adv}(x^{n-1})$ indicates the gradient of the adversarial loss \mathcal{L}_{adv} with respect to the input x^{n-1} .

3.2. Video Defense Framework for 3D Field-based TFG

Currently, there is still a lack of research on portrait defense under video-based conditions. A straightforward approach

is to apply existing image-based defense algorithms[8, 20, 21, 33, 42] frame by frame. However, this strategy suffers from several limitations: (1) the 2D perturbations generated by existing methods hardly remain effective in 3D space; (2) compression and resizing during video transmission often degrade or completely remove the added perturbations; and (3) even a one-minute video may contain thousands of frames, making frame-wise protection computationally prohibitive, typically requiring tens of hours to complete.

Unlike image-based TFG methods that synthesize video frames sequentially based on the input portrait image, personalized TFG models require only the user-specified driving conditions—such as camera viewpoint and guiding audio (or text)—once the model is trained. Therefore, previous end-to-end optimization approaches that add 2D perturbations directly to reference images are no longer effective in this setting.

Considering that obtaining accurate 3D information from the preprocessed reference video is crucial for achieving high-quality outputs, we instead target the **reference video processing stage** of the 3D field-based model for our defense. To address the aforementioned challenges, we propose a **video-level defense framework** consisting of the following key components, as demonstrated in Fig 2 .

3.2.1. Similarity-guided Parameter Sharing Mechanism

Compared with image defense, portrait video requires processing thousands of portrait frames for just one minute of content. Therefore, a practically useful video defense framework must improve its computational efficiency. By utilizing the high similarity between consecutive video frames, we design a parameter sharing strategy to accelerate optimization, as illustrated in Fig 2 (a). Specifically, the perturbation for the current frame is initialized by inheriting the optimized perturbation from the previous frame, weighted proportionally to their inter-frame similarity:

$$\delta_{initial}^{t+1} = SSIM(x^{t+1}, x^t) * \delta^t + \delta_{random} \quad (6)$$

Where x^t represents the frame of the time t .

3.2.2. Dual-domain Attention Mechanism with Multi-scale

Previous studies have shown that, compared to the spatial domain, the spectral characteristics of an image are more resilient to scale variations and color compression [11, 46]. Considering the introduction of the Multiscale Defense module, unlike previous approaches, we introduce perturbations in the frequency domain, as illustrated in Fig 2 (b1). Such perturbations can be effectively preserved across different scales, which significantly simplifies the optimization problem and improves efficiency, as demonstrated in our experiments. Furthermore, as illustrated in Fig 2 (b2), since arbitrary modifications in the frequency domain correspond to global perturbations in the spatial domain, a spatial

attention mechanism is incorporated to suppress redundant noise and enhance visual quality:

$$x' = \mathcal{F}^{-1}(\mathcal{F}(x) + \delta) \odot \mathbf{A}_{\text{spatial}} + x \quad (7)$$

Where x denotes the original image and x' is the updated image after perturbation. $\mathcal{F}(\cdot)$ and $\mathcal{F}^{-1}(\cdot)$ represent the Fourier and inverse Fourier transforms, respectively. δ is the perturbation added in the frequency domain, and $\mathbf{A}_{\text{spatial}}$ is the spatial attention matrix that adaptively suppresses redundant noise. The operator \odot denotes the element-wise multiplication, which modulates the reconstructed spatial signal with spatial attention.

During video transmission, scale variations frequently occur, which pose significant challenges to conventional defense algorithms, as demonstrated in the supplementary materials. To address this issue, losses at multiple scales are incorporated into our framework, as illustrated in Fig 2 (b3). Specifically, we adopt scale factors of 2 \times , 1.5 \times , 1 \times , 0.75 \times , and 0.5 \times as optimization objectives during implementation. Experimental results further validate the effectiveness and cross-scale generalization of this design on out-of-distribution resolutions, as illustrated in Table 1. The Multiscale defense loss can be described as:

$$\mathcal{L}_{\text{m.seg}}(x) = \sum_{s \in \mathcal{S}} \mathbb{E}_{(x,y) \sim \mathcal{D}} \left[\frac{1}{|M|} \sum_{(i,j) \in M} \log \left(1 - \sum_{c \in \mathcal{C}_{\text{tgt}}} P_{\theta}(c | R_s(x + \delta))_{i,j} + \epsilon \right) \right] \quad (8)$$

Where $\mathcal{S} = \{2.0, 1.5, 1.0, 0.75, 0.5\}$ represents the set of scaling factors. For each scale s , $R_s(\cdot)$ resizes the perturbed image $x + \delta$. $P_{\theta}(c | R_s(x + \delta))_{i,j}$ indicates the predicted probability of class c at pixel (i, j) from the segmentation model f_{θ} . Although facial classification results are used as the optimization objective, the resulting perturbations are still effective for other video processing pipelines, as illustrated in the appendix. \mathcal{C}_{tgt} is the set of target classes to be suppressed, and M denotes the binary mask defining the region of interest. The logarithmic term penalizes pixels where the target-class probability is high, thus encouraging misclassification within the masked region. A small ϵ is added for numerical stability.

3.2.3. Perceived quality enhanced

Compared to single-image scenarios, maintaining temporal coherence in videos requires higher image quality during the defense process. To this end, we employ a pretrained VGG [36] network to extract visual features from the defended images and align them with those of the original images during optimization, thereby enhancing the perceptual quality of the defended results:

$$\mathcal{L}_{\text{sem}}(x, y) = \sum_{l \in \mathcal{L}} w_l \frac{1}{N_l} \|\phi_l(x) - \phi_l(y)\|_2^2, \quad (9)$$

Where $\phi_l(\cdot)$ represents the activation map of the l -th selected VGG16 layer, and $\mathcal{L} = \{3, 8, 15, 22\}$ denotes the set of feature layers used to capture hierarchical semantic information. w_l is the layer-specific weight that gradually decreases with network depth, emphasizing low-level texture alignment. Empirically, we set its value as $[1.0, 0.75, 0.5, 0.25]$. N_l is the total number of feature elements in layer l .

The entire adversarial example generation process using the PGD algorithm can be described as follows:

$$\mathcal{L}_{\text{vdf.adv}}(x, y) = \mathcal{L}_{\text{sem}}(x, y) - \mathcal{L}_{\text{m.seg}}(x) \quad (10)$$

$$x^n = \mathcal{P}_{B_{\infty}(x, \delta)} [x^{n-1} - \eta \text{sign}(\nabla_{x^{n-1}} \mathcal{L}_{\text{vdf.adv}}(x^{n-1}, y))] \quad (11)$$

4. Experiments

4.1. Experimental Setup

4.1.1. Implementation Details

In our experiments, We resized the video uniformly to 512 \times 512, following the standard experimental setup described in [19], without identity overlap. The reference videos were sampled at 25 FPS and the audio was sampled at 16 kHz. We utilized the publicly available SyncTalk [28] model as the talking-head generation method, together with its accompanying video processing pipeline commonly used in the field [5, 17, 19, 28, 35, 39, 43]. Experimental results for other models are mentioned in the appendix. The maximum perturbation per pixel was set to 0.05 and the process ended when the misclassifications rate on five predefined scales exceeded 80%. Over 500 hours are conducted of experiments on four RTX A6000 GPUs.

Baselines and Dataset. We collected 11 videos from previous works as our dataset [19, 28, 44]. The proposed method with five state-of-the-art privacy-protection approaches, including AdvDM[21], PhotoGuard[33], Mist[20], SDS[42], and Silencer-I[8] are compared. To evaluate the performance of the baselines while considering time and energy costs, we extracted 45-second segments from each video as reference videos.

4.1.2. Metrics

The quality of the protected and generated videos was evaluated using the following metrics:

Image Quality. Peak Signal-to-Noise Ratio (PSNR), Structural Similarity Index Measure (SSIM), and Fréchet Inception Distance (FID) [13] were utilized to assess the quality of the protected videos and their corresponding generated video frames.

Audio-Visual Synchronization. The confidence score of SyncNet [30] was used to evaluate audio-visual synchro-

Method	SSIM(GT) \uparrow	PSNR(GT) \uparrow	FID(GT) \downarrow	Sync(GT) \uparrow	M-LMD(GT) \downarrow	Time Cost
AdvDM(-)[21]	0.4793	27.48	63.40	7.8606	2.6537	22.28h
AdvDM(+)[42]	0.5111	27.25	121.62	7.9172	2.7631	25.90h
PhotoGuard[33]	0.5040	26.54	107.53	7.6222	3.1085	18.60h
Mist[20]	0.5093	26.64	108.08	7.6225	3.0570	27.15h
SDS(+)[42]	0.5453	27.57	127.02	7.9264	2.7472	12.68h
SDS(-)[42]	0.5477	28.55	67.31	7.8797	2.6503	12.82h
SDST(-)[42]	0.5530	27.55	100.80	7.7968	2.9659	19.47h
Silencer-I[8]	0.5311	28.48	78.29	7.8652	2.6416	18.75h
VDF (ours)	0.9063	33.43	45.33	7.9397	2.2968	0.27h(\times 47)
Ground Truth	1.00	∞	0.00	8.0789	0.0000	-

Table 1. Quantitative Comparisons with State-of-the-art Methods on GT

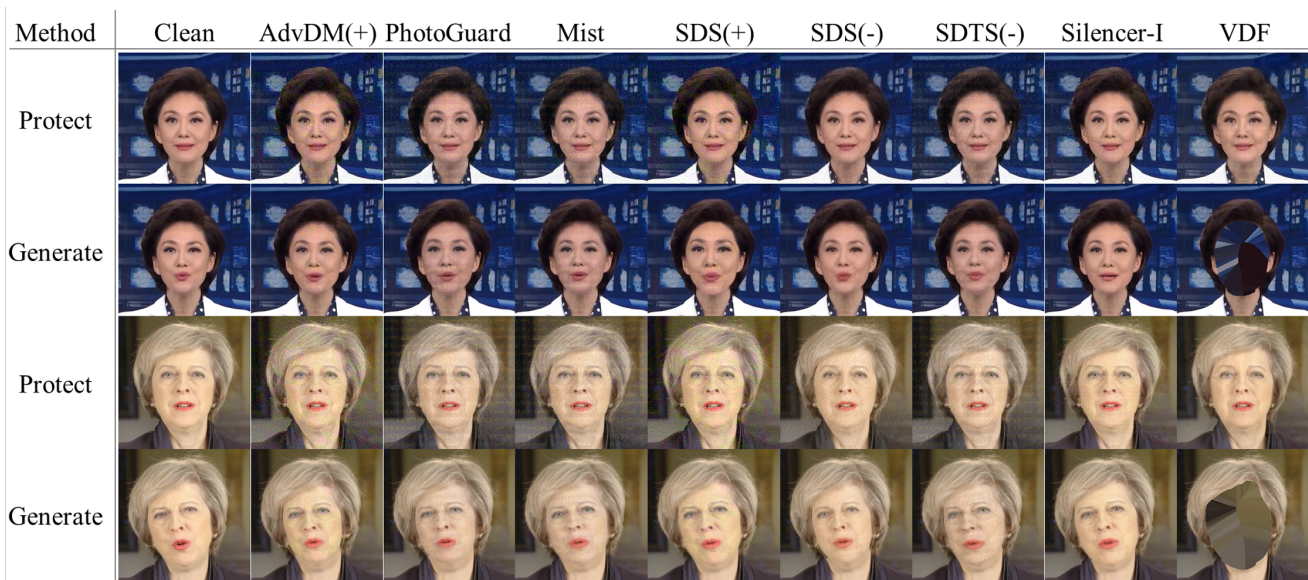


Figure 4. Qualitative Comparison with Image Protection Methods.

Method	SSIM \downarrow	PSNR \downarrow	FID \uparrow	Sync \downarrow	M-LMD \uparrow
AdvDM(-)[21]	0.8999	29.58	21.15	6.7968	9.7250
AdvDM(+)[42]	0.8820	28.53	57.84	6.7685	9.5517
PhotoGuard[33]	0.8890	27.58	39.67	6.0465	16.7003
Mist[20]	0.8949	28.53	40.41	6.0717	13.9059
SDS(+)[42]	0.8864	29.01	61.50	6.8855	9.0316
SDS(-)[42]	0.8973	28.49	19.57	6.7258	12.0642
SDST(-)[42]	0.8309	25.68	61.29	6.4674	13.1509
Silencer-I[8]	0.8983	29.59	30.36	6.7450	10.0228
VDF(ours)	0.8547	16.78	174.88	0.1700	∞
Ground Truth	1.00	∞	0.00	8.1076	0.0000

Table 2. Quantitative Comparisons with State-of-the-art Methods on generated videos by SyncTalk

nization in both protected and generated videos. Additionally, the mouth landmark distance (M-LMD) [3] was employed to indicate the consistency of speech content.

4.2. Protected Video Metrics

We first compare the effectiveness of VDF in preserving video quality against other methods. Using 11 videos of 45 seconds each as reference videos, we applied state-of-the-art protection methods and computed metrics between the protected and original reference videos.

As shown in Table 1, our method achieves the best results across all metrics, demonstrating its superior ability to retain the visual information of the original video. Notably, compared to the best baseline, our method improves SSIM and FID by 63% and 28.5%, respectively. Furthermore, our method offers a substantial improvement in computational

Method	Protected	JPEG	Resize	Diffpure	Freqpure
	PSNR/FID/M-LMD	PSNR↓/FID↑/M-LMD↑	PSNR↓/FID↑/M-LMD↑	PSNR↓/FID↑/M-LMD↑	PSNR↓/FID↑/M-LMD↑
AdvDM(-)[21]	30.55/22.09/8.34	29.30/18.38/8.25	28.73/24.34/11.28	29.63/20.32/7.82	29.44/24.16/8.10
AdvDM(+)[42]	27.25/67.21/8.26	26.78/59.78/8.78	28.52/48.62/11.62	28.25/20.45/8.53	27.77/23.30/8.92
PhotoGuard[33]	25.96/45.98/7.46	28.10/35.12/8.92	24.82/56.62/22.62	26.73/19.47/8.54	25.36/21.95/10.56
Mist[20]	28.54/44.65/7.72	26.35/36.48/7.83	23.50/101.77/47.17	26.63/18.02/9.06	26.95/20.98/11.23
SDS(+)[42]	29.72/73.09/8.39	27.53/58.82/7.40	28.83/50.08/10.18	28.95/19.90/8.47	29.25/22.43/9.16
SDS(-)[42]	28.00/23.57/8.16	30.18/16.57/7.67	28.48/28.40/12.81	29.53/20.17/8.31	29.11/22.97/9.37
SDST(-)[42]	26.44/42.61/7.54	28.08/24.62/7.92	27.06/46.03/14.48	28.91/17.67/8.16	27.05/19.59/9.87
Silencer-I[8]	30.77/30.32/8.22	29.52/17.35/7.40	28.76/25.97/11.17	28.94/16.20/7.50	29.43/23.13/8.34
VDF(ours)	15.65/206.79/∞	25.29/68.80/14.23	16.05/168.02/196.09	30.37/16.23/7.39	28.87/21.02/8.09

Table 3. Quantitative Comparisons with State-of-the-art Methods on generated vedios by SyncTalk based on pured images

efficiency. It reduces the protection time for a 45-second video from several hours to just 0.27 hours.

4.3. Privacy Protection Performance

As shown in Table 2, the videos generated from the videos protected from baseline maintain high scores in SSIM, Sync, and M-LMD, indicating that these protection methods fail against SyncTalk-based generation. Note that when training SyncTalk on VDF-protected videos, the preprocessing step fails to extract any meaningful information, leading to training collapse. This confirms the effectiveness of our method in privacy protection. For quantitative comparison, we adopted the pipeline from SyncTalk, where we preserved the non-generated regions of the reference video and filled the facial areas with background content. This processed video served as the generated output for metric computation. Furthermore, due to the absence of facial regions, the M-LMD metric could not be computed and was therefore set to ∞ . Qualitative results in Fig. 4 show that, unlike methods requiring significant perturbations, our approach maintains visual consistency while effectively preventing SyncTalk from extracting subject privacy information.

4.4. Anti-Purification Experiments

We evaluate four purification methods—JPEG [34], Resize [41], DiffPure [23], and FreqPure [26]—by training and testing SyncTalk on the purified videos. As shown in Table 3, VDF achieves the best performance under JPEG and Resize purification, benefiting from its frequency-domain perturbations and multi-scale robustness that are difficult to remove. VDF performs slightly worse than baseline methods against DiffPure and FreqPure, since those baselines introduce much stronger facial perturbations that purification cannot fully eliminate. Notably, although VDF adds smaller perturbations, the generated identities still deviate significantly from the protected ones, reflecting a trade-off between visual quality and robustness to purification.

Noise Domain	Spatial Mask	VGG	Init Noise	Protected Image			
				SSIM	PSNR	FID	Time Cost
Spatial	–	✓	✓	0.9786	44.77	14.70	135min
Frequency	–	✓	✓	0.9554	32.24	39.12	44min
Frequency	✓	–	✓	0.8955	33.17	50.67	15min
Frequency	✓	✓	–	0.9326	33.42	33.74	485min
Frequency	✓	✓	✓	0.9063	33.43	45.33	16min

Table 4. Progressive ablation study

4.5. Ablation Study

We evaluated the impact of different noise domains and individual components on both the quality of protected images and the computational time cost. As shown in Table 4, while spatial domain noise yields better image quality, it also incurs the higher time cost. In contrast, frequency domain noise achieves a threefold improvement in efficiency over spatial noise. Building on this, incorporating a spatial mask further enhances protection efficiency without significantly compromising visual quality. The VGG semantic loss helps maintain the visual quality of protected videos by limiting the distortion caused by frequency domain perturbations.

For the configuration without noise inheritance, due to its substantial computational demand, we tested on a subset of three videos, observing an average processing time of 485 minutes. In comparison, the introduction of noise inheritance significantly accelerates the generation of adversarial examples, making it feasible to protect full-length videos against SyncTalk-based generation.

5. Conclusion

We propose a dual-domain attention-based video defense framework that protects portrait privacy from 3D-field personalized TFG models. By combining frequency-domain perturbations with adaptive spatial attention and parameter sharing mechanism, our method achieves high visual quality, robustness to scaling and purification, and superior efficiency in real-world privacy defense. In future work, we aim to develop a unified video defense framework capable of simultaneously countering privacy threats posed by

both image-referenced and video-referenced TFG models.

References

- [1] ShahRukh Athar, Zexiang Xu, Kalyan Sunkavalli, Eli Shechtman, and Zhixin Shu. Rignerf: Fully controllable neural 3d portraits. In *Proceedings of the IEEE/CVF Conference on Computer Vision and Pattern Recognition (CVPR)*, pages 20364–20373, New Orleans, LA, 2022. IEEE. 1, 3
- [2] Lele Chen, Zhiheng Li, Ross K. Maddox, Zhiyao Duan, and Chenliang Xu. Lip movements generation at a glance. In *Proceedings of the European Conference on Computer Vision (ECCV)*, pages 520–535. Springer, 2018. 3
- [3] Lele Chen, Ross K. Maddox, Zhiyao Duan, and Chenliang Xu. Hierarchical cross-modal talking face generation with dynamic pixel-wise loss. In *Proceedings of the IEEE/CVF Conference on Computer Vision and Pattern Recognition (CVPR)*, pages 7832–7841, 2019. 7
- [4] Lele Chen, Ross K. Maddox, Zhiyao Duan, and Chenliang Xu. Hierarchical cross-modal talking face generation with dynamic pixel-wise loss. In *Proceedings of the IEEE/CVF Conference on Computer Vision and Pattern Recognition (CVPR)*, pages 7832–7841, 2019. 3
- [5] Kyusun Cho, Jounghbin Lee, Heeji Yoon, Yeobin Hong, Jaehoon Ko, Sangjun Ahn, and Seungryong Kim. Gaus-siantalker: Real-time high-fidelity talking head synthesis with audio-driven 3d gaussian splatting. In *Proceedings of the 32nd ACM International Conference on Multimedia (ACM MM)*, pages 10985–10994. ACM, 2024. 1, 3, 6
- [6] Jiankang Deng, Jia Guo, Niannan Xue, and Stefanos Zafeiriou. Arcface: Additive angular margin loss for deep face recognition. In *Proceedings of the IEEE/CVF Conference on Computer Vision and Pattern Recognition (CVPR)*, pages 4690–4699, 2019. 1
- [7] Yilun Du and Igor Mordatch. Implicit generation and modeling with energy based models. *Advances in neural information processing systems*, 32, 2019. 3
- [8] Yuan Gan, Jiayu Miao, Yunze Wang, and Yi Yang. Silence is golden: Leveraging adversarial examples to nullify audio control in ldm-based talking-head generation. In *Proceedings of the IEEE/CVF Conference on Computer Vision and Pattern Recognition (CVPR)*, 2025. 1, 5, 6, 7, 8
- [9] Will Grathwohl, Kuan-Chieh Wang, Jörn-Henrik Jacobsen, David Duvenaud, Mohammad Norouzi, and Kevin Swersky. Your classifier is secretly an energy based model and you should treat it like one. *arXiv preprint arXiv:1912.03263*, 2019. 3
- [10] Jiatao Gu, Lingjie Liu, Peng Wang, and Christian Theobalt. Stylenerf: A style-based 3d-aware generator for high-resolution image synthesis. In *Proceedings of the International Conference on Learning Representations (ICLR)*, 2022. 1
- [11] Chuan Guo, Jared S. Frank, and Kilian Q. Weinberger. Low frequency adversarial perturbation. In *Proceedings of The 35th Uncertainty in Artificial Intelligence (UAI)*, pages 1127–1137. PMLR, 2020. 2, 5
- [12] Yudong Guo, Keyu Chen, Sen Liang, Yong-Jin Liu, Hujun Bao, and Juyong Zhang. Ad-nerf: Audio driven neural radiance fields for talking head synthesis. In *Proceedings of the IEEE/CVF International Conference on Computer Vision (ICCV)*, pages 10104–10113. IEEE, 2021. 1, 3
- [13] Martin Heusel, Hubert Ramsauer, Thomas Unterthiner, Bernhard Nessler, and Sepp Hochreiter. Gans trained by a two time-scale update rule converge to a local nash equilibrium. In *Advances in Neural Information Processing Systems (NeurIPS)*, 2017. 6
- [14] Mitch Hill, Jonathan Mitchell, and Song-Chun Zhu. Stochastic security: Adversarial defense using long-run dynamics of energy-based models. *arXiv preprint arXiv:2005.13525*, 2020. 3
- [15] Jaehwan Jeong, Seunghyun Lee, Jaeho Kim, Minjung Park, Junghyun Choi, and Sungmin Kim. Faceshield: Defending facial image against deepfake threats. In *Proceedings of the IEEE/CVF International Conference on Computer Vision (ICCV)*, 2025. 2
- [16] Zhe Kong, Feng Gao, Yong Zhang, Zhuoliang Kang, Xiaoming Wei, Xunliang Cai, Guanying Chen, and Wenhan Luo. Let them talk: Audio-driven multi-person conversational video generation. *arXiv preprint arXiv:2505.22647*, 2025. 1
- [17] Jiahe Li, Jiawei Zhang, Xiao Bai, Jun Zhou, and Lin Gu. Efficient region-aware neural radiance fields for high-fidelity talking portrait synthesis. In *Proceedings of the IEEE/CVF International Conference on Computer Vision (ICCV)*, pages 7568–7578. IEEE, 2023. 3, 6
- [18] Jiahe Li, Jiawei Zhang, Xiao Bai, Jin Zheng, Xin Ning, Jun Zhou, and Lin Gu. Talkinggaussian: Structure-persistent 3d talking head synthesis via gaussian splatting. In *European Conference on Computer Vision (ECCV)*, pages 127–145. Springer Nature Switzerland, 2024. 1, 3
- [19] Jiahe Li, Jiawei Zhang, Xiao Bai, Jin Zheng, Jun Zhou, and Lin Gu. Instag: Learning personalized 3d talking head from few-second video. In *Proceedings of the IEEE/CVF Conference on Computer Vision and Pattern Recognition (CVPR)*, pages 10690–10700, Los Alamitos, CA, 2025. IEEE. 3, 6, 1
- [20] Chumeng Liang and Xiaoyu Wu. Mist: Towards improved adversarial examples for diffusion models. *arXiv preprint arXiv:2305.12683*, 2023. 1, 5, 6, 7, 8
- [21] Chumeng Liang, Xiaoyu Wu, Yang Hua, Jiaru Zhang, Yiming Xue, Tao Song, Zhengui Xue, Ruhui Ma, and Haibing Guan. Adversarial example does good: Preventing painting imitation from diffusion models via adversarial examples. In *Proceedings of the 40th International Conference on Machine Learning (ICML)*, pages 20763–20786. PMLR, 2023. 1, 5, 6, 7, 8
- [22] Aleksander Madry, Aleksandar Makelov, Ludwig Schmidt, Dimitris Tsipras, and Adrian Vladu. Towards deep learning models resistant to adversarial attacks. *arXiv preprint arXiv:1706.06083*, 2017. 5
- [23] Weili Nie, Brandon Guo, Yujia Huang, Chaowei Xiao, Arash Vahdat, and Animashree Anandkumar. Diffusion models for adversarial purification. In *Proceedings of the 39th International Conference on Machine Learning (ICML)*, pages 16805–16827. PMLR, 2022. 1, 2, 3, 8

- [24] Omkar Parkhi, Andrea Vedaldi, and Andrew Zisserman. Deep face recognition. In *BMVC*, 2015. 1
- [25] Gaozheng Pei, Ke Ma, Yingfei Sun, Qianqian Xu, and Qingming Huang. Diffusion-based adversarial purification from the perspective of the frequency domain. *arXiv preprint arXiv:2505.01267*, 2025. 3
- [26] Gaozheng Pei, Ke Ma, Yingfei Sun, Qianqian Xu, and Qingming Huang. Diffusion-based adversarial purification from the perspective of the frequency domain. *arXiv preprint arXiv:2505.01267*, 2025. 1, 2, 3, 8
- [27] Xiangyu Peng, Zangwei Zheng, Chenhui Shen, Tom Young, Xinying Guo, Binluo Wang, Hang Xu, Hongxin Liu, Mingyan Jiang, Wenjun Li, Yuhui Wang, Anbang Ye, Gang Ren, Qianran Ma, Wanying Liang, Xiang Lian, Xiwen Wu, Yuting Zhong, Zhuangyan Li, Chaoyu Gong, Guojun Lei, Leijun Cheng, Limin Zhang, Minghao Li, Ruijie Zhang, Silan Hu, Shijie Huang, Xiaokang Wang, Yuanheng Zhao, Yuqi Wang, Ziang Wei, and Yang You. Open-sora 2.0: Training a commercial-level video generation model in \$200 k. *arXiv preprint arXiv:2503.09642*, 2025. 1
- [28] Ziqiao Peng, Wentao Hu, Yue Shi, Xiangyu Zhu, Xiaomei Zhang, Hao Zhao, Jun He, Hongyan Liu, and Zhaoxin Fan. Synctalk: The devil is in the synchronization for talking head synthesis. In *Proceedings of the IEEE/CVF Conference on Computer Vision and Pattern Recognition (CVPR)*, pages 666–676, Seattle, WA, 2024. IEEE. 1, 2, 3, 6
- [29] Ziqiao Peng, Wentao Hu, Junyuan Ma, Xiangyu Zhu, Xiaomei Zhang, Hao Zhao, Hui Tian, Jun He, Hongyan Liu, and Zhaoxin Fan. Synctalk++: High-fidelity and efficient synchronized talking heads synthesis using gaussian splatting. *arXiv preprint arXiv:2506.14742*, 2025. 3
- [30] K. R. Prajwal, R. Mukhopadhyay, V. P. Nambodiri, and C. V. Jawahar. A lip sync expert is all you need for speech to lip generation in the wild. In *Proceedings of the 28th ACM International Conference on Multimedia (ACM MM)*, pages 484–492, Seattle, WA, 2020. ACM. 6
- [31] K. R. Prajwal, Rudrabha Mukhopadhyay, Vinay P. Nambodiri, and C. V. Jawahar. A lip sync expert is all you need for speech to lip generation in the wild. In *Proceedings of the 28th ACM International Conference on Multimedia (ACM MM)*, pages 484–492. Association for Computing Machinery, 2020. 3
- [32] Zuomin Qu, Zuping Xi, Wei Lu, Xiangyang Luo, Qian Wang, and Bin Li. Df-rap: A robust adversarial perturbation for defending against deepfakes in real-world social network scenarios. *IEEE Transactions on Information Forensics and Security*, 19:3943–3957, 2024. 2
- [33] Hadi Salman, Alaa Khaddaj, Guillaume Leclerc, Andrew Ilyas, and Aleksander Madry. Raising the cost of malicious ai-powered image editing. *arXiv preprint arXiv:2302.06588*, 2023. 1, 5, 6, 7, 8
- [34] Pedro Sandoval-Segura, Jonas Geiping, and Tom Goldstein. Jpeg compressed images can bypass protections against ai editing. *arXiv preprint arXiv:2304.02234*, 2023. 1, 2, 3, 8
- [35] Shuai Shen, Wanhua Li, Zheng Zhu, Yueqi Duan, Jie Zhou, and Jiwen Lu. Learning dynamic facial radiance fields for few-shot talking head synthesis. In *European conference on computer vision*, 2022. 3, 6
- [36] Karen Simonyan and Andrew Zisserman. Very deep convolutional networks for large-scale image recognition. In *Proceedings of the International Conference on Learning Representations (ICLR)*, 2015. 6
- [37] Yang Song and Stefano Ermon. Generative modeling by estimating gradients of the data distribution. *Advances in neural information processing systems*, 32, 2019. 3
- [38] Rui-Qing Sun, Haoran Li, Jiabin Wang, Ming Chen, Yutong Zhao, Wenrui Zhang, and Jing Liu. Is it truly necessary to process and fit minutes-long reference videos for personalized talking face generation? *arXiv preprint arXiv:2511.xxxxx*, 2025. 1
- [39] Jiaxiang Tang, Kaisiyuan Wang, Hang Zhou, Xiaokang Chen, Dongliang He, Tianshu Hu, Jingtuo Liu, Gang Zeng, and Jingdong Wang. Real-time neural radiance talking portrait synthesis via audio-spatial decomposition. *arXiv preprint arXiv:2211.12368*, 2022. 3, 6
- [40] Run Wang, Ziheng Huang, Zhikai Chen, Li Liu, Jing Chen, and Lina Wang. Anti-forgery: Towards a stealthy and robust deepfake disruption attack via adversarial perceptual-aware perturbations. 2
- [41] Cihang Xie, Jianyu Wang, Zhishuai Zhang, Zhou Ren, and Alan Yuille. Mitigating adversarial effects through randomization. *arXiv preprint arXiv:1711.01991*, 2017. 3, 8
- [42] Haotian Xue, Chumeng Liang, Xiaoyu Wu, and Yongxin Chen. Toward effective protection against diffusion-based mimicry through score distillation. In *Proceedings of the International Conference on Learning Representations (ICLR)*, 2023. 1, 5, 6, 7, 8
- [43] Shunyu Yao, RuiZhe Zhong, Yichao Yan, Guangtao Zhai, and Xiaokang Yang. Dfa-nerf: Personalized talking head generation via disentangled face attributes neural rendering. *arXiv preprint arXiv:2201.00791*, 2022. 3, 6
- [44] Zhenhui Ye, Ziyue Jiang, Yi Ren, Jinglin Liu, Jinzheng He, and Zhou Zhao. Geneface: Generalized and high-fidelity audio-driven 3d talking face synthesis. In *Proceedings of the Eleventh International Conference on Learning Representations (ICLR)*, 2024. 1, 2, 3, 6
- [45] Jongmin Yoon, Sung Ju Hwang, and Juho Lee. Adversarial purification with score-based generative models. In *International Conference on Machine Learning*, pages 12062–12072. PMLR, 2021. 3
- [46] Jiawei Zhang, Qiang Yi, Di Lu, and Jun Sang. Low-mid adversarial perturbation against unauthorized face recognition system. *Information Sciences*, 648:119566, 2023. 2, 5
- [47] Jiawei Zhang, Jiahe Li, Xiaohan Yu, Lei Huang, Lin Gu, Jin Zheng, and Xiao Bai. Cor-gs: Sparse-view 3d gaussian splatting via co-regularization. In *Proceedings of the European Conference on Computer Vision (ECCV)*, pages 335–352, Cham, Switzerland, 2024. Springer Nature Switzerland. 3
- [48] Zhengyue Zhao, Jinhao Duan, Kaidi Xu, Chenan Wang, Rui Zhang, Zidong Du, Qi Guo, and Xing Hu. Can protective perturbation safeguard personal data from being exploited by stable diffusion? In *Proceedings of the IEEE/CVF Conference on Computer Vision and Pattern Recognition (CVPR)*, pages 24398–24407, 2024. 1

Efficient and Robust Video Defense Framework against 3D-field Personalized Talking Face

Supplementary Material

6. More Implementation Details

Considering the computational cost of the experiments, we selected three subjects with different skin tones and genders from previous work [19, 28, 38, 44] as evaluation targets in Section 4.4 and the subsequent experiments. In all experiments, we strictly follow the official settings of SyncTalk [28] and Instag[19], and use the AVE module as the audio encoder as reported in their papers to ensure high-fidelity performance.

7. More Experiments

7.1. More Anti-Purification Experiments

To evaluate the purification resistance of our method, a face recognition model is employed to measure how effectively the purified results distort the subject’s identity. Widely used face recognition models, VGG-Face [24] and ArcFace [6], are employed to extract facial features from the generated video frames. The Euclidean distance between the feature vectors of the ground truth and the generated frames is computed to assess identity consistency. The quantitative results in the Table 5 and Fig 5 indicate that VDF successfully distorts the target identity and achieves purification robustness comparable to state-of-the-art methods, even though it is not specifically designed to defend against purification models.

Method	Diffpure		Time Cost
	VGG-Face↑/ArcFace↑	VGG-Face↑/ArcFace↑	
AdvDM(-)[21]	0.3259/0.2442	<u>0.3497</u> /0.2964	22.28h
AdvDM(+)[42]	0.3227/0.2850	0.3534/ <u>0.2867</u>	25.90h
PhotoGuard[33]	0.3771 /0.3184	0.4458 /0.3768	18.60h
Mist[20]	0.3751/ 0.3307	0.3814/0.3098	<u>27.15h</u>
SDS(+)[42]	<u>0.2996</u> /0.2452	0.3788/0.2908	12.68h
SDS(-)[42]	0.3098/ <u>0.2315</u>	0.3902/0.3262	12.82h
SDST(-)[42]	0.3480/0.2904	0.4345/ 0.3841	19.47h
Silencer-I[8]	0.3308/0.2549	0.3991/0.3661	18.75h
VDF(ours)	0.3157/0.2369	0.3649/0.3413	0.27h (× 47)

Table 5. Quantitative Comparisons with State-of-the-art Methods on generated vedios by Syncntalk based on pured images. The underlined values indicate the worst performance, while the bold values denote the best performance.

7.2. Perturbations Scale Analysis

To investigate the impact of different perturbation scales, we tested various maximum perturbation bounds b (i.e., $|\delta| \leq b$), where

$$b \in \{0, 0.05, 0.10, 0.15, 0.20, 0.25, 0.30, 0.35\}.$$

The qualitative results are shown in Fig. 6. The experiments demonstrate that as the perturbation magnitude increases, the performance of non-target facial processing modules progressively degrades and eventually collapses.

7.3. Evaluating the Transferability of VDF

Method	SSIM↓	PSNR↓	FID↑	Sync↓	M-LMD↑
AdvDM(-)[21]	0.8434	26.53	18.29	6.4403	7.0307
AdvDM(+)[42]	0.8248	25.48	33.97	6.4232	7.2869
PhotoGuard[33]	0.8282	24.89	24.84	6.5805	7.2397
Mist[20]	0.8264	24.82	27.13	6.7106	7.3441
SDS(+)[42]	0.8193	25.59	41.84	6.6785	7.2548
SDS(-)[42]	0.8439	26.14	17.71	6.5763	6.8721
SDST(-)[42]	0.8344	25.35	22.67	6.8172	7.1875
Silencer-I[8]	0.8418	26.30	18.14	6.5448	6.9969
VDF(ours)	0.7243	14.80	219.46	∞	101.50
Ground Truth	1.00	∞	0.00	8.1076	0.0000

Table 6. Quantitative Comparisons with State-of-the-art Methods on generated videos by Instag

To assess the transferability of VDF, we conducted a cross-model evaluation. Specifically, we first optimize the adversarial noise on the exquisite processing modules of SyncTalk [28], which is based on a NeRF architecture, and then evaluate it on the Instag [19] model, which is built upon a 3DGS framework. These two models belong to two distinct types of 3D-field architectures.

As shown in Table 6 and Fig 7, the synchronization values of the generated videos indicate that VDF retains strong adversarial effects even on models that were not used during optimization. Although VDF is designed as a white-box attack, these results demonstrate its remarkable generalization ability across different 3D-field TFG models. This cross-model robustness suggests promising potential for broader applicability and further validates the effectiveness of our method.

A plausible explanation for this phenomenon lies in two key factors: (1) the 3D-field TFG models share some similar exquisite process modules, and (2) more importantly, they all rely on the exquisite processing of reference videos, which is exactly the component targeted by VDF. This shared module dependency likely introduces common vulnerabilities that VDF is able to exploit across models, leading to its consistent adversarial performance.

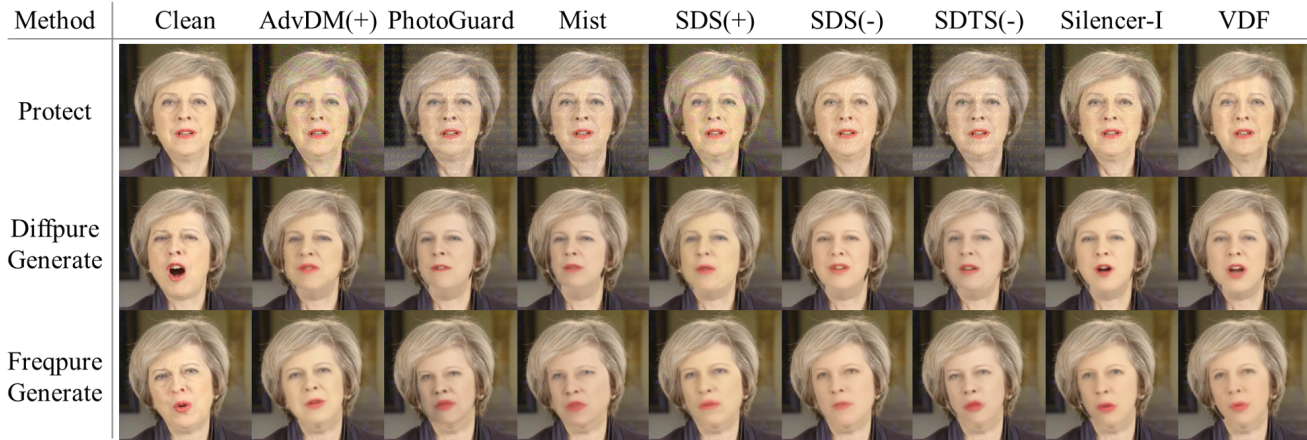


Figure 5. Qualitative Comparison of images generated after Diffpure and Freqpure purification with Image Protection Methods.

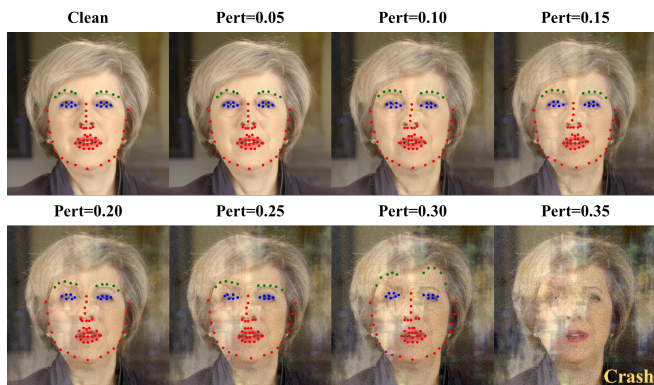


Figure 6. Impact of Perturbation Scale on Facial Landmark Detection.

Method	SSIM↓	PSNR↓	FID↑	Sync↓	M-LMD↑
FaceShield[15]	0.9241	29.93	6.48	8.3298	7.9563
DFRAP[32]	0.9228	30.96	15.13	8.3691	7.6121
AntiForgery[40]	0.9185	29.86	10.93	8.1812	7.4437
VDF(ours)	0.8547	16.78	174.88	0.1700	∞
Ground Truth	1.00	∞	0.00	8.1076	0.0000

Table 7. Quantitative Comparisons with State-of-the-art deepfake Methods on generated videos by syntalk

7.4. Comparison Against Deepfake Defense Baselines

To further evaluate the effectiveness of the proposed VDF framework, we compare it against three widely used Deepfake defense methods — FaceShield [15], DFRAP [32], and AntiForgery [40]. As shown in Table 7 and Fig 8, all baselines achieve relatively high SSIM and PSNR scores, indicating that their perturbations are overly conservative

and preserve facial structures, which allows SyncTalk to successfully extract 3D identity information from the reference frames. In contrast, VDF achieves a significantly lower SSIM (0.8547) and PSNR (16.78), suggesting that the exquisite data process was severely disrupted.

Regarding generative performance under adversarial defense, VDF exhibits a substantially higher FID score (174.88), meaning the generated videos deviate more strongly from the original identity, which corroborates the success of our defense. Moreover, VDF achieves the lowest Sync score (0.1700), which indicates strong disruption of audio-driven identity extraction. Although M-LMD is theoretically unbounded under heavy distortions, its divergence under VDF confirms that fine-grained lip synchrony is severely broken, thus preventing realistic talking-face reconstruction.

Overall, VDF demonstrates superior capability in blocking identity reconstruction during personalized TFG generation, while existing Deepfake defense baselines struggle to prevent SyncTalk from producing high-quality forged videos. These results highlight the necessity of video-level defense targeting 3D field-based TFG models rather than conventional Deepfake methods.

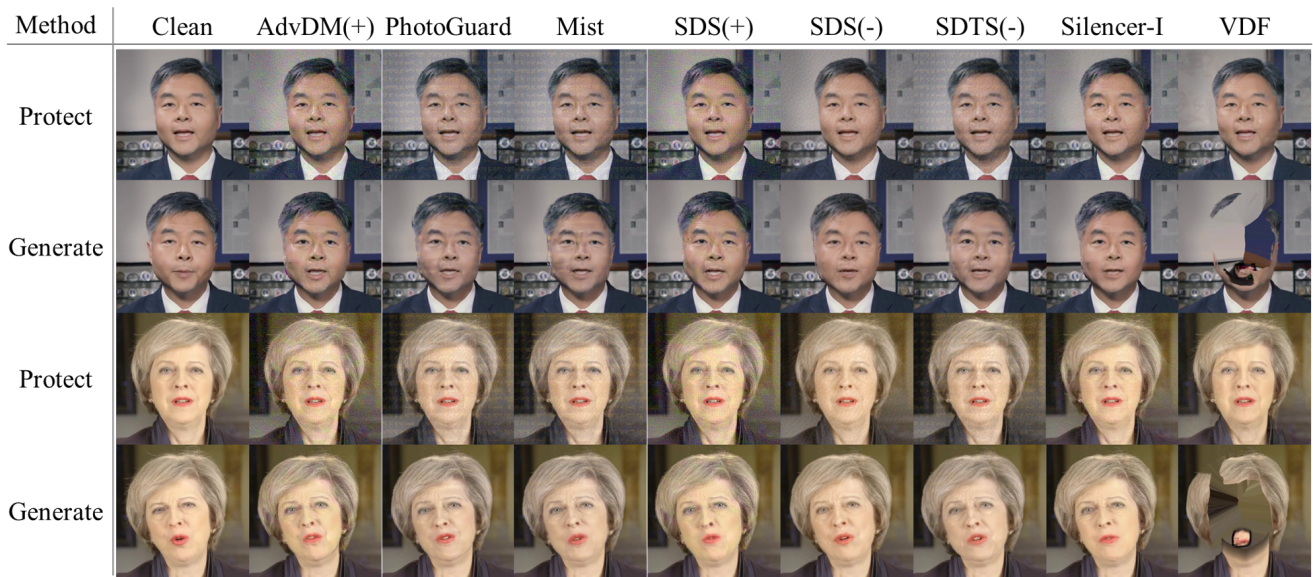


Figure 7. Qualitative Comparison with Image Protection Methods on Instag.

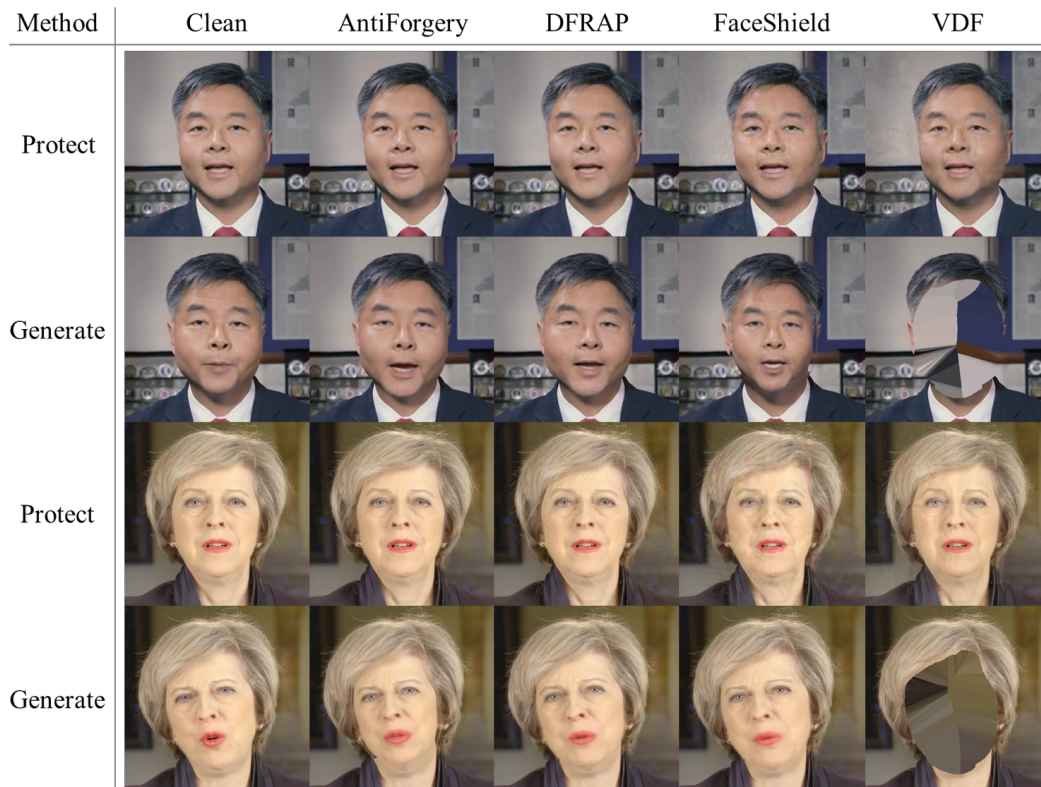


Figure 8. Qualitative Comparison with Deepfake Protection Methods.